System Analysis of Thermochemical-Based Biorefineries for Coproduction of Hydrogen and Electricity

Robert J. Braun
Luke G. Hanzon
Jered H. Dean

Department of Engineering,
Colorado School of Mines,
Golden, CO 80401

Fuels derived from biomass feedstocks are a particularly attractive energy resource pathway given their inherent advantages of energy security via domestic fuel crop production and their renewable status. However, there are numerous questions regarding how to optimally produce, distribute, and utilize biofuels such that they are economically, energetically, and environmentally sustainable. Comparative analyses of two conceptual 2000 tons/day thermochemical-based biorefineries are performed to explore the effects of emerging technologies on process efficiencies. System models of the biorefineries, created using ASPEN Plus®, include all primary process steps required to convert a biomass feedstock into hydrogen, including gasification, gas cleanup and conditioning, hydrogen purification, and thermal integration. The biorefinery concepts studied herein are representative of "near-term" (approximately 2015) and "future" (approximately 2025) plants. The near-term plant design serves as a baseline concept and incorporates currently available commercial technologies for all nongasifier processes. Gasifier technology employed in these analyses is centered on directly heated, oxygen-blown, fluidized-bed systems that are pressurized to nearly 25 bars. The future plant design employs emerging gas cleaning and conditioning technologies for both tar and sulfur removal unit operations. A 25% increase in electric power production is observed for the future case over the baseline configuration due to the improved thermal integration while realizing an overall plant efficiency improvement of 2 percentage points. Exergy analysis reveals that the largest inefficiencies are associated with the (i) gasification, (ii) steam and power production, and (iii) gas cleanup and purification processes. Additional suggestions for improvements in the biorefinery plant for hydrogen production are given.
[DOI: 10.1115/1.4003541]

1 Introduction

The pathways for production of primarily transportation fuels from biomass feedstocks are numerous and varied in both type of fuel (e.g., alcohols, liquid hydrocarbons, kerosene, and synthetic gases) and level of technology maturation. Thermochemical conversion of biomass to fuel and power generally occurs through either pyrolysis or gasification. Pyrolysis is the thermochemical decomposition of biomass in the absence of oxygen. It produces a mixture of synthesis gas (syngas) and bio-oil at temperatures around 500°C. Gasification uses partial oxidation of the feedstock to provide heat for the reactor and is typically run at temperatures above 800°C. The higher temperature produces syngas with very little bio-oil (which is considered an impurity or tar). Gasification is a particularly promising alternative for the production of second generation bio-fuels from nonfood, cellulosic biomass.

The focus of the present work is on production of gaseous hydrogen and electricity via directly heated, thermochemical conversion of ligno-cellulosic biomass. This pathway centers on gasification of biomass to generate a syngas (i.e., H_2/CO-rich) that is cleaned, purified, and pressurized for hydrogen transport and/or storage. In particular, the present study compares the performance of two 2000 tons/day (tPD) biorefinery plant concepts supplied with woody biomass from both energetic and exergetic viewpoints. The two biorefinery plant design concepts studied herein are representative of "near-term" (approximately 2015) and "future" (approximately 2025) cases, the process designs of which are based on numerous considerations related to hardware performance capabilities and technology readiness assessments.

The objectives of the present work are to (i) develop biorefinery system models that adequately capture plant performance characteristics; (ii) analyze the thermodynamic performance of baseline and advanced biorefinery concepts on energetic and exergetic bases, including quantification of the performance gains associated with improved system thermal integration obtained from employment of advanced gas cleanup processes; and (iii) identify areas for additional system performance improvements.

In this paper, previous work in thermodynamic analyses of biorefineries and gasification are discussed first, followed by an overview on biomass resource availability and plant sizing. The biomass gasifier is the heart of the system and thus, a more in-depth overview of the gasifier performance modeling is presented. A description of the two biorefinery concepts is then given, followed by a summary of energetic and exergetic plant performance. The study concludes with a discussion of additional areas for improvement and a summary of conclusions.

2 Previous Work

Previous work in system analyses of hydrogen production from biomass gasification includes that of Larson et al. [1], Spath et al. [2], Williams et al. [3], Corradetti and Desideri [4], and Dean et al. [5,6]. Both Spath et al. and Corradetti and Desideri focused on indirectly heated atmospheric pressure biomass gasification systems, yet the technologies, unit operations, and economics given in these works are directly relevant to the present effort.

Contributed by the Advanced Energy Systems Division of ASME for publication in the JOURNAL OF ENERGY RESOURCES TECHNOLOGY. Manuscript received August 4, 2010; final manuscript received January 19, 2011; published online March 29, 2011. Assoc. Editor: Professor Nesrin Ozalp.

Their works employed indirectly heated gasification, which is a two-stage, fluidized-bed process where the heat needed for reaction is produced by burning char in a separate chamber to heat a synthetic olivine "sand." The hot sand is then circulated through the reaction chamber to provide the thermal energy necessary to drive endothermic gasification reactions. The gasification reactions make use of steam to both stabilize the entrained flow of biomass and olivine and to assist in the chemical decomposition of biomass components into a syngas made up of primarily H_2, CO, CO_2, CH_4, and tars. In particular, the syngas cleanup technologies, such as tar mitigation and desulfurization, employed by Spath et al. provide the basis for use of the LO-CAT process in this study. Larson et al. [1] examined the coproduction of hydrogen and electricity from switchgrass with *N*th generation pressurized, directly heated gasification systems at the 5000 tPD scale and is inclusive of modeling approaches, energetic performance estimates, and process technologies. Williams et al. [3] explored the technology, economics, and environmental aspects of producing CH_3OH and H_2 from biomass for fuel cell vehicle applications. The work compared different gasification technologies, especially in relation to fuel production from other primary resources, such as natural gas and coal. Recent studies on the production of ethanol and mixed alcohols from biomass have been performed using both indirect and direct gasification technologies [7,8]. These studies indicate that indirect gasification may be preferred for alcohol production (from an economic perspective) due to the high cost of the air separation unit, which provides the oxygen needed for directly-heated gasifier operation. Nevertheless, Dutta and Phillips [8] also acknowledged that directly-heated gasifier technology may be preferred for synthetic fuels production where higher H_2:CO ratios are required in fuel synthesis, for example, for Fischer–Tropsch and methanol liquids. The present work differs from these prior studies in its feedstock type (and in some cases gaseous hydrogen product), biorefinery scale, use of different, emerging gas cleanup technologies, and its focus on exergetic analysis of the biorefinery.

Exergetic analyses of gasification plants have roots that reach back to the first energy "crisis" in the 1970s [9,10]. While such early studies focused on coal gasification and the production of synthetic natural gas, the methods for exergy property calculations and analysis results on analogous plant unit operations (such as fluidized-beds, syngas cleanup, and air separation processes) are highly relevant to biomass gasification system analysis. As reported in these early studies, exergy destructions in coal gasification plants are principally found to reside with steam, power, oxygen, and syngas (i.e., gasification) generation processes. More recently, exergetic analyses of biomass gasification systems [11–13] have taken a theoretical slant aimed at gaining a thermodynamic understanding of the impact that operating parameters and feedstock type have on biomass gasification. These studies focus on the gasifier-alone as the largest single inefficiency device within the system and typically assume a condition of equilibrium in the gasifier outlet syngas. Recommendations for gasifier operating conditions and feedstock pretreatments are made. In actual fluidized-bed biomass gasifiers, the relatively low operating temperatures (800–900°C) and short reactor residence times (1–3s [14]) produce syngas compositions far from chemical equilibrium [3].

3 Biomass Type and Plant Size

Recent assessments have shown that an excess of 400×10^6 tons of biomass are currently available per year in the United States [15]. Some estimates predict that as much as 1 billion tons of biomass could be available in the future with changes to land management and agricultural practices [16]. The primary ligno-cellulosic feedstock types of interest for thermochemical conversion are agricultural residues, wood residues, and dedicated energy crops. Agricultural residues include plant waste products that are not needed for animal feed or erosion control on farms and ranches. Wood residues are composed of wood produced by forest maintenance, and urban wood residues, such as pallets and mill residues. Both types of residue feedstock are available today but the infrastructure for collection and delivery is not widely available.

Table 1 Biomass ultimate analysis

	Dry (wt %)	As Received (wt %)
Carbon	50.2	46.7
Hydrogen	6.06	5.6
Oxygen	40.4	37.6
Nitrogen	0.6	0.56
Sulfur	0.02	0.02
Chlorine	0.01	0.009
Ash	2.71	2.5
Water	–	6.9
HHV (kJ/kg)	19,022	17711
LHV (kJ/kg)	17,700	16312

Use of a dedicated energy crop was assumed in this analysis to provide homogeneous feed properties. Wood chips were chosen over native grasses because of biomass drying and feeding concerns associated with fibrous grasses. The biomass feedstock used in this analysis is untreated hybrid poplar wood chips where feedstock compositional data were obtained from the Phyllis biomass properties database [17], and an ultimate analysis is given in Table 1 in terms of the organic fraction (C, H, O, N, S, Cl), ash, and moisture contents. The low moisture content of the biomass (6.9 wt %) means that drying will not be required before feed preparation or gasification. Other studies have reported moisture content of farmed trees as high as 50 wt % [2]. Drying (and therefore energy) requirements are highly dependent on moisture and the feedstock type.

Selection of biorefinery size is a nontrivial task and is dependent on achieving both proper economy-of-scale and cost-effective supply of biomass to the plant. Establishment of optimal biorefinery size is often carried out employing biofuel supply chain models and due to refinery cost scaling parameters, such models typically recommend the maximum allowable plant size based on resource availability [18,19]. Plant capacity in this effort was guided by geographic information system (GIS) data from a previous study by Dean et al. [5], which recommend a 2000 tPD refinery size. Assuming an 80 km (50 mile) collection radius, there are multiple locations throughout the country that could support this level of wood requirement. At scales larger than 2000 tPD, the number of possible plant locations in the United States becomes substantially limited [5,15]. Additionally, at these large plant sizes, economy-of-scales are more favorable in terms of minimizing unit production costs. However, this conclusion is often based on the assumption of using the same technology as the larger plants (for example, air separation units) for which cost scaling factors are highly nonlinear. It is quite possible that the use of emerging technologies, such as water-gas shift membrane reactors, ion transport membranes, warm gas desulfurization, or other hardware may enable better low-end economy-of-scales for smaller (<1000 tPD) biorefineries [20,21].

4 Biorefinery Process Overview

Figure 1 depicts a high-level process flow diagram of a biorefinery plant. Biomass is typically prepared for gasification through drying to remove moisture (not necessary here), milling the feedstock to the appropriate particle size, and pressurization to gasifier operating conditions in lock-hoppers. Following gasification, syngas cooling, cleanup, and water-gas shift operations proceed before the cleaned hydrogen-rich gas is further purified via pressure-swing adsorption (PSA). The final hydrogen product is compressed to 700 bars for transport and any unconverted fuel is

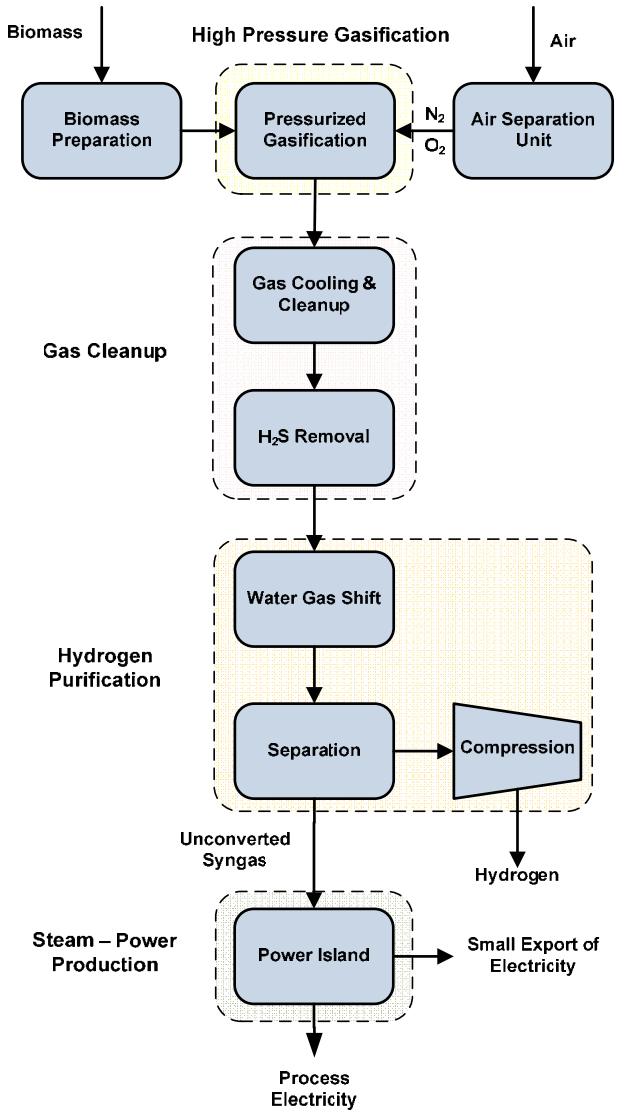

Fig. 1 Biorefinery process flow diagram

burned to generate steam and power for onsite use. Any excess electricity generated is exported to the utility grid. The biorefinery concepts developed and analyzed in this study focus on technologies that are either near term or advanced. The near-term plant design in this study serves as a baseline concept and is defined as employing hardware and process technologies that are commensurate with the 2015 timeframe, which implies hardware demonstration at either pilot or commercial scales. While there are many biomass gasifier types under development, only a single gasifier technology was evaluated in this work given the complexity of the plant. The advanced future plant design employs emerging gas cleaning and conditioning technologies for both tar and sulfur removal unit operations and does not focus on alternative gasification technologies.

In biomass gasification systems, syngas clean up consists of tar removal/reduction, scrubbing and filtration, desulfurization, and hydrogen purification. In general, several stages of tar reduction and removal are required for fluidized-bed type gasification (as opposed to entrained-flow reactors in which tar is completely destroyed or converted in the gasifier, substantially reducing the gas clean up train of the plant). The steps involved in tar mitigation are (i) primary reduction via O_2 selective oxidation of tar in the gasifier freeboard, followed by secondary methods in (ii) a dolomite guard bed, (iii) tar cracking in a fixed bed reformer, and (iv) either water scrubbing or use of a catalytic candle filter.

Development of desulfurization technology is in flux with emerging sulfur-tolerant water-gas shift catalysts and warm gas desulfurization reactors. Commercial technology, such as LO-CAT, is not capable of removing H_2S as effectively as the Rectisol or Selexol processes, but is significantly more economical. The major disadvantage of employing a LO-CAT desulfurization approach is with system thermal integration as the syngas must be cooled to 60°C before entering the LO-CAT unit and then reheated for the downstream sulfur polishing step. Warm (or also referred to as "hot") gas desulfurization technology is promising and chosen for its thermal integration attributes in the future-case design concept.

The clean syngas is synthesized to higher concentrations of hydrogen primarily through water-gas shift reactors (high and low temperatures) and finally with pressure-swing adsorption. Interestingly, if water-gas shift catalysts are tolerant to sulfur (e.g., via Haldor-Topsoe type SSK commercial shift catalyst), then pressure-swing adsorption units can theoretically admit syngas containing 80–100 ppmv levels of H_2S without deleterious effects on PSA performance and purify the final hydrogen production gas.

4.1 Biomass Gasification. Pressurized biomass gasification is not yet a commercial technology for refinery-scale fuel production but has been demonstrated at pilot plant scales. Gasification of biomass shares many of the same processes and technologies associated with commercial coal gasification, which has been proven with multiple large-scale installations throughout the world. As discussed in the literature review section of this paper, both indirectly-heated (atmospheric pressure) and directly-heated (pressurized) gasification technologies are advancing. Indirectly-heated gasification technology is perhaps most commonly associated with that developed by Battelle Columbus Laboratory (the process is now licensed by SilvaGas) that consists of two fluid-bed reactors that thermally communicate via a hot circulating sand. Recently, the fast internal circulating fluid-bed (FICFB) process was developed as another indirectly-heated gasification approach that separates the steam gasification of biomass from the char combustion process to deliver a reasonably high calorific syngas (~12 MJ/N m^3) [22,23]. It accomplishes this with a quasi-circulating fluidized-bed process via a chute that connects the gasification with the combustion sections. This technology has been commercially demonstrated at small scale (~42 tPD). The Choren process is an entrained-flow biomass gasifier type that has also reached commercial demonstration status and is most like a coal gasifier. In this process, the biomass feedstock undergoes a pyrolysis step first and is then followed by char gasification at high temperature and pressure using oxygen and steam [22].

Unlike these systems, the gasifier type employed in the present work is centered on directly-heated, oxygen-blown, fluidized-bed reactors operating at elevated pressure. Operating at high pressure increases the overall plant efficiency and decreases tar production. Unfortunately, due to ash agglomeration, the bed temperature cannot be as hot as entrained-flow gasifier types, such as those frequently found in coal gasification. The lower bed temperature results in nonequilibrium syngas compositions and significant tar production.

The gasifier technology selected for this biorefinery systems analysis is derived from the Institute of Gas Technology (IGT) process research unit (PRU) that was developed during the 1980s [24]. The PRU was a 12 tPD directly-heated, steam and oxygen blown, fluidized-bed pressurized gasifier. The gasifier design concept employed herein differs from the original PRU in that dual lock-hopper and secondary oxygen injection systems have been added. By switching to the dual lock-hopper system, it is estimated that only 0.15 kg of nitrogen gas will be needed per kilogram of biomass for pressurization of the biomass feed. A bed temperature of 860°C was chosen so that primary tars would be

Table 2 Gasifier model inputs and parameters

Inputs	Parameters	Parameter value
Biomass proximate, ultimate and sulfur analysis	Lock-hopper N_2-gas pressurization requirement	0.15 $kg_{N_2}/kg_{biomass}$ N_2-to-biomass ratio (as received)
Gasifier pressure (24 bars)	H_2/CO ratio of product syngas	1.43:1.0
Temperature, pressure and flow rate of biomass	Mole fractions of CH_4, C_2H_6, and C_2H_4 in syngas	CH_4:7.4% C_2H_6: 0.2% C_2H_4:0.18%
Fluidized bed temperature (860°C) [a]	Tar production	1.6 wt % of biomass feed
Freeboard temperature (1030°C) [a]	Heat loss	1% of biomass LHV
	Steam-to-dry biomass ratio	0.8 kg/kg

[a]Established by oxygen mass flow to gasifier.

completely cracked inside the bed but ash agglomeration could be kept to a minimum. Bed temperature can be set by controlling the mass flow of oxygen supplied to the gasifier. Secondary oxygen supplied from the air separation unit is injected into the freeboard of the gasifier to facilitate reduction of secondary and tertiary tar compounds [25]. Based on extensive literature review, it is estimated that at a freeboard syngas outlet temperature of 1030°C, an 88% decrease in tar content and a 60% reduction in ammonia are achievable. The freeboard outlet temperature of 1030°C is not expected to cause additional ash agglomeration since the injection takes place well above the fluidized-bed. Catalytic bed materials were not used in the gasifier design concept because the effect of operating parameters in combination with partial oxidation is not well understood in the extant literature.

4.2 Gasifier Modeling. The gasifier was modeled in ASPEN Plus® plant simulation software. One challenge in modeling fluidized-bed gasification of biomass is that the raw syngas produced is not of equilibrium composition. Furthermore, the reaction kinetics involved in biomass gasification are poorly understood. Thus, numerous unit operations and empirically based constraint equations were necessary to adequately model gasifier operation. A total of 9 individual unit operations and 11 FORTRAN calculator blocks were needed to model the gasifier reaction chamber. The modeling technique was based on the approach given by Larson et al. [1], with parameter adjustments to match published GTI experimental results. The components employed within ASPEN consisted of a combination of different reactors in which the entering biomass solid is first decomposed into its elemental components using the proximate and ultimate analyses of the biomass. A second reactor sets the amount of tar formed based on experimental results. The biomass stream is then passed to an equilibrium reactor where it is mixed with steam, oxygen, and nitrogen (from lock-hopper pressurization) to convert the biomass solid into a syngas. Constraints on equilibrium are made based on experimental data from the PRU. Subsequent reactors within ASPEN are used to accomplish the tar reduction via secondary oxygen injection and adjustment of the final H_2:CO ratio in the raw syngas. Separators within the gasifier model are used to remove ash and char from the syngas. The required numerical inputs and empirically based parameters are detailed in Table 2.

Several assumptions regarding chemical conversion and heat loss are made from empirical data and are incorporated into the gasifier model. Based on a regression of the PRU data done by Bain [26], it is assumed that 1.6 wt % of the bone dry biomass feed is converted to tar in the gasifier bed. In addition, the model assumes 100% carbon conversion even though the empirical regression predicts 2.7% carbon loss to char. This assumption was made based on benchmarking results that showed model syngas flow rates were too low if char production was allowed. Heat loss from the gasifier is estimated at 1% of the lower heating value (LHV) of the raw biomass entering the gasifier. Finally, the total water to bone dry biomass ratio in the gasifier is held constant at 0.8 based on the average value reported in the PRU experimental results. Tars are generally defined as compounds formed during gasification that have a molecular weight greater than that of benzene (C_6H_6) [14]. Rather than attempt to predict and track multiple hydrocarbons, anthracene ($C_{14}H_{10}$) was used as the single representative compound to model tar. Its usage provides a good average composition in terms of both molecular weight and heating value of primary, secondary, and tertiary tar compounds found in gasifier syngas [14,27].

4.3 Gasifier Model Benchmarking. The ASPEN Plus® gasifier model output was benchmarked against two published cases, which encompass both baseline and future gasification plants in this study. The first comparison was made with the results that are representative of the future case as published by Larson et al. [1]. The second point of comparison was the GTI empirical regression published by Bain [26]. For both comparisons, the inputs and feedstock were changed to exactly match those published. The model results were then compared in terms of both flow and composition and, in general, were found to be within 1% of published data. Deviations with Larson et al. that exceeded 1% were related to syngas outlet temperature (1030°C versus 1014°C) and minor differences in the aromatic content of the syngas. The model differed from the GTI regression in both char yield and gas volume. The GTI regression predicts that approximately 2.7% of the dry ash-free biomass will produce char rather than syngas. The ASPEN Plus® model developed here assumes 100% char conversion (i.e., no char production) and so the variation is expected.

A cryogenic air separation unit (ASU) is used to produce oxygen at 95% purity. In addition to producing oxygen, a nitrogen stream of 97% purity is available as a byproduct from the ASU and a portion of it is used as the inert pressurization agent for the lock-hopper system, with the balance vented to the atmosphere. According to literature sources, 260–350 kW h of electricity are needed for every ton of oxygen produced [28,29]. A conservative value of 350 kW h/ton of oxygen was assumed. This value does not include compression of the oxygen and nitrogen product gases, which exit the ASU at approximately 1.5 bars and must be raised to a pressure sufficiently high to enter the gasifier operating at 24 bars.

4.4 Plant Description. A detailed plant process flow diagram for the baseline design concept is depicted in Fig. 2. Wood chips are milled to the appropriate gasifier feed particle size, consuming some 300 kW of electrical energy in the process and then enter the plant at station (1). The biomass is pressurized in the lock-hopper with nitrogen from the ASU (station 27) and then fed via screws into the gasifier. High pressure oxygen (25) and steam (20) are injected and served to fluidize the bed and provide the oxidant for partial oxidation of the biomass and steam for temperature moderation via endothermic reforming of the intermediate methane species that are produced from gasification reactions. Secondary oxygen injection (26) consumes a large fraction of the tars produced in the fluidized-bed and raises the syngas temperature from 860°C to 1030°C. Ash and large particulate are removed from the syngas in the cyclone and the syngas (2) is then delivered to secondary tar reduction unit operations.

The tar removal portion of the plant consists of two catalytic tar cracking reactors followed by a wet scrubbing step. The first reactor contains a packed bed of dolomite, which has catalytic properties that aid in the reforming of tar compounds. This stage is important because it reduces the tar to levels, which are safe for the more sensitive Ni-based catalysts found in the second tar cracking reactor. Wang et al. [30] determined that to protect the

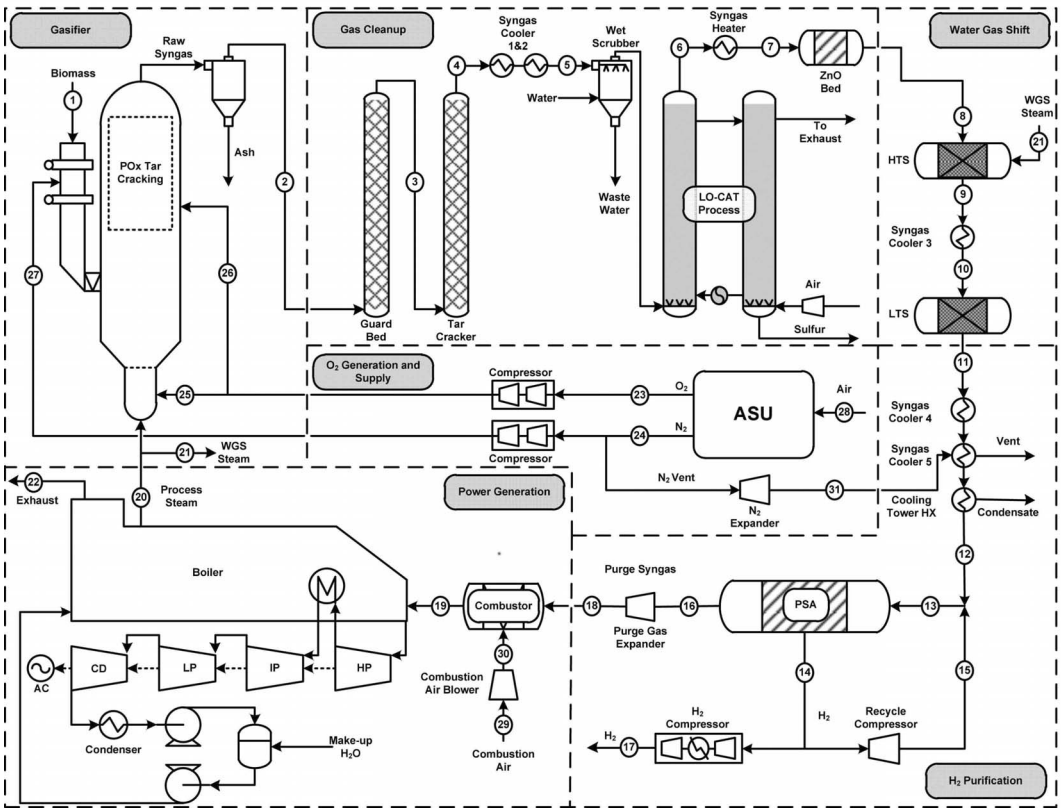

	T (°C)	P(bar)	m(kg/s)
1	25	1.0	23.1
2	1030	22.0	50.4
3	1028	22.0	50.4
4	693	21.0	50.4
5	161	21.0	50.4
6	40	20.0	35.4
7	375	20.0	35.4
8	375	20.0	35.4
9	444	19.0	50.0
10	200	19.0	50.0
11	264	19.0	50.0
12	40	17.0	41.9
13	41	17.0	44.0
14	41	17.0	3.8
15	41	17.0	2.1
16	41	2.0	40.2
17	60	70.0	1.7
18	4	1.2	40.2
19	890	1.2	105.7
20	334	25.0	31.1
21	334	25.0	14.6
22	90	1.0	105.7
23	10	1.5	7.4
24	10	1.5	29.5
25	254	25.0	5.8
26	254	25.0	1.6
27	281	25.0	3.5
28	25	1.0	36.9
29	25	1.0	65.5
30	35	1.15	65.5
31	-17	1.05	26.0

Fig. 2 Baseline-case biorefinery process flow diagram

reforming catalysts from excessive deactivation, tar concentrations should be less than 10 g/Nm^3 at the inlet of the reforming reactor. Tar conversion in the dolomite guard bed is set such that a tar concentration of approximately 8 g/Nm^3 is achieved before entry into the tar cracking unit. The tar cracker envisioned in this plant design is a fixed bed reactor filled with a Ni-based catalyst that reforms the majority of the remaining tar to hydrogen and carbon monoxide before the final tar mitigation step of wet scrubbing. However, the syngas must first be cooled to about 160°C in a series of heat exchangers (4) before being passed into the spray tower (5) where tars, ammonia, and any remaining particulates are removed to the required purity level.

After wet scrubbing the remaining impurity of concern is H_2S. Since cocapture of CO_2 is not an objective in this plant concept (although as discussed later, it can substantially affect efficiency performance), the LO-CAT process followed by a zinc oxide (ZnO) polishing bed was determined to be the most economical H_2S remediation method. The LO-CAT process is not capable of removing H_2S to the <1 ppmv required for fuel synthesis so ZnO polishing beds are needed to ensure that the purity requirements are met.

The tar and sulfur-free syngas (8) then passes through a two-stage adiabatic water-gas shift (WGS) process. Steam from the heat recovery steam generator is injected at a molar ratio of 3:1 into the clean syngas, which is then delivered to the first stage. The first WGS reactor operates adiabatically with an inlet temperature of 375°C and is followed by a low-temperature stage operating nominally at 230°C. The operating conditions of the WGS reactors were specified to maximize the production of H_2 for downstream separation and export.

The H_2 rich stream (12) is then processed through a PSA unit where the H_2 is separated from the other constituent gases (14) and is either recycled (15) to boost H_2 partial pressure at the PSA inlet or is pressurized to 70 bars for export (17). The remaining syngas is sent to the boiler (16) to produce steam.

The heating and cooling needs of the plant are met through a network of heat exchangers, which are designed to maximize heat recovery and utilize the recovered heat to produce steam for on-site power production. Syngas coolers 1–4 are integrated into the heat recovery steam generator (HRSG) system, while heat recovered in syngas cooler 5 and the cooling tower heat exchanger is lost to the environment. The matching of heating and cooling streams was accomplished through the application of pinch analysis techniques [31]. This was done to maximize the amount of heat recovered in the system and improve plant efficiency. The steam produced by the cooling of process streams is fed to a four-stage steam turbine set that produces a gross power of nearly 35 MW.

4.5 Plant Performance. The baseline-case performance is summarized in Table 3. Approximately 410 MW (higher heating value (HHV) of biomass energy are supplied to the biorefinery and about 237 MW of hydrogen and 15 MW of net electrical power are produced, resulting in a total plant efficiency of 61.6% HHV (57.2% LHV). Internal auxiliary power in the plant amounts to about 22 MW of which the ASU and O_2/N_2 compression is responsible for over half of the total. The next largest auxiliary power consumers are related to hydrogen compression and the steam plant cooling tower that provides condenser cooling water (not shown in Fig. 2).

5 Future-Case Concept

5.1 Plant Description. The future-case concept explores the impact of emerging gas cleanup technologies on system efficiency performance. A process flow diagram of the future-case concept is depicted in Fig. 3 and differs from the baseline-case in two main ways. First, to improve the thermal integration of the plant, it was desired that process gas cooling and reheat steps associated with

Table 3 Biorefinery performance summary

	Baseline case	Future case
Energy inputs		
Feedrate (kg/s)	23.14	23.14
Biomass LHV (MJ/kg)	16.31	16.31
Biomass HHV (MJ/kg)	17.71	17.71
Biomass energy input (MW), LHV	377.4	377.4
Biomass energy input (MW), HHV	409.8	409.8
Plant outputs (MW)		
Hydrogen output (ton/h)	6.01	6.01
H_2 energy output, LHV	200.8	200.8
H_2 energy output, HHV	237.4	237.4
Electricity power output steam cycle	34.78	46.80
N_2 and purge expanders	2.33	2.33
Gross output (H_2+power), LHV	237.9	252.4
Gross output (H_2+power), HHV	274.6	289.4
Internal power use (MW)		
Air separation unit	9.22	9.22
Oxygen compressor	2.43	2.43
Nitrogen compressor	1.50	1.50
Biomass prep	0.30	0.30
Lock-hopper	0.32	0.32
LO-CAT/HGDS comp	0.01	0.02
PSA Recycle compressor	0.13	0.28
H_2 compressor	4.33	4.33
Cooling tower (fan, pumps)	1.62	2.10
Boiler feedwater pumps	1.14	1.42
Combustion air compressor	1.02	1.02
Other auxiliary power	0.12	0.12
Total internal power use	22.14	23.06
Net electric power out	14.97	26.07
Net energy output, LHV	215.7	226.8
Net energy output, HHV	252.4	263.5
Efficiency		
Fuel efficiency, HHV	57.9%	57.9%
Electrical efficiency, HHV	3.7%	6.4%
Total plant efficiency, HHV	61.6%	64.3%
Total plant efficiency, LHV	57.2%	60.1%

the wet scrubbing and LO-CAT processes be eliminated. For wet scrubbing to be effective, the process gas must be cooled below the saturation temperature to prevent the gas from flashing the scrubbing water to steam. This requires extensive cooling since the syngas leaving the tar cracker is at approximately 700°C. The LO-CAT process also requires the inlet gas to be cooled to approximately 60°C. The ZnO polishing beds that are required to achieve the <1 ppmv H_2S concentration require that the syngas stream be reheated to 375°C. To avoid cooling and reheat, the Future-case concept employs a catalytic candle filter operating near 700°C to replace the wet scrubbing process. A traditional sintered metal or ceramic candle filter is packed with a reforming catalyst that converts any remaining tar to H_2 and CO. Laboratory-scale tests with laboratory-produced synthesis gas have reported conversion efficiencies as high as 100% for secondary tars [32].

The second difference between the baseline- and future-case models is the replacement of the catalytic redox LO-CAT process with warm gas desulfurization (WGDS). This technology is being developed in integrated gasification combined cycle (IGCC) systems and integrates well with the temperature profile of the syngas cleanup subsystem. The WGDS requires much less cooling than the LO-CAT process and operates at high temperature (450–500°C versus 60°C) [33].

5.2 Plant Performance. Future-case biorefinery efficiency performance is improved by 2.3 percentage points over the baseline-case through the integration of advanced gas cleanup technology into the process. As shown in Table 3, the fuel efficiency (i.e., hydrogen production efficiency) is about the same at 57.9%, but about 12 MW of additional electric power are produced which yields an increase in electrical efficiency of nearly 3%. An overall total plant efficiency of 64.3% HHV (60.1% LHV) is obtained.

6 Thermodynamic Analysis Approach

While energetic performance assessments are helpful and necessary, an exergetic analysis is more revealing and quantitatively insightful toward understanding the location and magnitude of process inefficiencies within the plant. In the following, exergy analysis is employed on the baseline and future cases, and an examination of each plant concept is carried out in terms of exergy destructions and efficiencies within their respective subsystems.

6.1 Exergy Property and Efficiency Estimates. Thermodynamic property evaluation for exergy of a substance largely follows the methods of Moran [34,35] and Szargut [36]. The reference environment chosen here is that of Szargut [37] or as also given by Moran and Shapiro [35] as "model II."

6.1.1 Physical Exergy. Physical (or thermomechanical) exergy is a measure of a nonreacting substance's departure from thermal and mechanical (i.e., pressure) equilibria with a reference environment. The specific physical exergy on a molar basis is expressed as

$$\bar{\psi}_p = \Delta\bar{h} - T_o\Delta\bar{s} \tag{1}$$

where

$$\Delta\bar{h} = \bar{h}_{T,P} - \bar{h}_{T_o,P_o} \tag{2}$$

$$\Delta\bar{s} = \bar{s}_{T,P} - \bar{s}_{T_o,P_o} \tag{3}$$

When considering an ideal gas mixture, the exergy of the mixture is the sum of the partial physical exergy of the constituents. It is expressed by

$$\bar{\psi}_{p,\text{mix}} = \sum_i y_i(\bar{h}_{T,P} - \bar{h}_{T_o,P_o} - T_o(\bar{s}_{T,P} - \bar{s}_{T_o,P_o})) \tag{4}$$

where y_i is the mole fraction of the ith component in the mixture, and enthalpy, $\bar{h}$ and entropy, $\bar{s}$ are evaluated using property data from ASPEN Plus®. For the solid state carbon and sulfur, the following approximations for $\Delta\bar{h}$ and $\Delta\bar{s}$ were used:

$$\Delta\bar{h} = \bar{c}_{p,\text{av}}(T - T_o) \tag{5}$$

$$\Delta\bar{s} = \bar{c}_{p,\text{av}} \ln\left(\frac{T}{T_o}\right) \tag{6}$$

6.1.2 Chemical Exergy. The specific chemical exergy of a substance is calculated according to

$$\bar{\psi}_{\text{ch,mix}} = \sum_i (\bar{\psi}_{\text{ch},i} + \bar{R}T_o \ln y_i) \tag{7}$$

The first term $\bar{\psi}_{\text{ch},i}$ is the specific chemical exergy of the ith pure component and the second term $\bar{R}T_o \ln y_i$ is a correction factor that accounts for the change in exergy of the pure component due to its presence in the mixture. The chemical exergy of the majority of the pure components was taken from Appendix III of Szargut [36]. The total exergy of the biomass feedstock was estimated from [35]

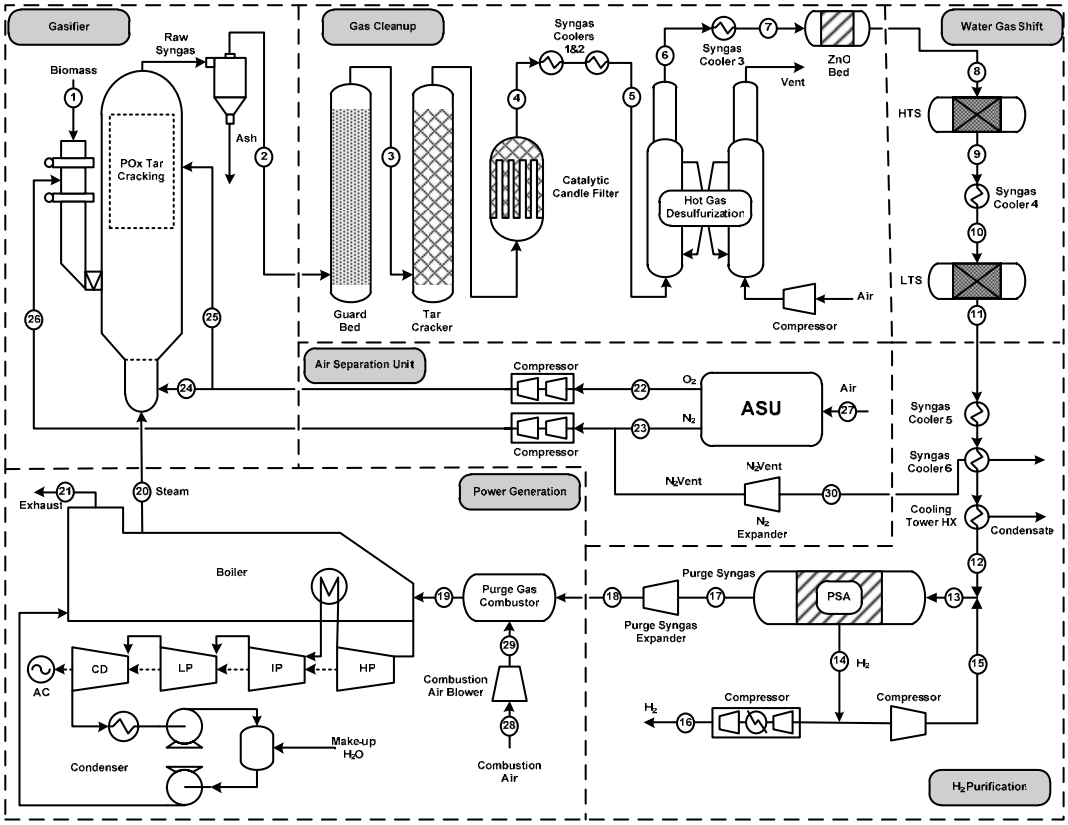

	T (°C)	P(bar)	m(kg/s)
1	25	1.0	23.1
2	1030	22.0	50.4
3	1028	21.7	50.4
4	693	21.0	50.4
5	500	21.0	50.4
6	500	20.0	50.4
7	375	20.0	50.4
8	375	19.0	50.4
9	459	19.0	50.4
10	200	18.0	50.4
11	266	18.0	50.4
12	40	17.0	41.9
13	44	16.0	44.1
14	42	15.0	3.8
15	51	16.0	2.1
16	60	70.3	1.7
17	43	2.0	40.3
18	18	1.1	40.3
19	890	1.1	105.8
20	334	25.0	16.5
21	95	1.0	105.8
22	10	1.5	7.4
23	10	1.5	1.6
24	254	25.0	5.8
25	254	25.0	1.6
26	281	25.0	3.5
27	25	1.0	36.9
28	25	1.0	65.5
29	35	1.15	65.5
30	-17	1.05	26.0

Fig. 3 Future-case process flow diagram

$$\psi_{\mathrm{ch}} = (\mathrm{LHV})_d\left(1.0438 + 0.0013\frac{h}{c} + 0.1083\frac{o}{c} + 0.0549\frac{n}{c}\right) + 6740s \tag{8}$$

where $(\mathrm{LHV})_d$ is the lower heating value of the dry biomass, h/c is the hydrogen to carbon ratio (mass), o/c is the oxygen to carbon ratio (mass), and n/c is the nitrogen to carbon ratio (mass), and s is the mass fraction of sulfur. The total specific exergy of the streams is the sum of the physical and chemical exergy of the mixture.

$$\bar{\psi}_{\mathrm{total,mix}} = \bar{\psi}_{p,\mathrm{mix}} + \bar{\psi}_{\mathrm{ch,mix}} \tag{9}$$

6.1.3 Exergetic Efficiency. Efficiency definitions are primarily a matter of consensus; i.e., an agreement over the purpose of the component or system is made such that the appropriate terms in the numerator and denominator can be entered. In the present analysis, the biorefinery was subdivided into seven primary subsystems:

1. gasifier
2. tar cleanup
3. H_2S cleanup
4. water-gas shift
5. H_2 purification and compression (PSA)
6. steam and power generation
7. air separation

Within each subsystem, the exergy inputs and outputs were calculated using the approach described above and from state point information provided by the ASPEN Plus® models. The second-law efficiency (η_{II}) was calculated according to the following:

$$\eta_{\mathrm{II}} = \frac{\sum \dot{\psi}_{\mathrm{useful,out}}}{\sum \dot{\psi}_{\mathrm{in}}} \tag{10}$$

7 Baseline-Case Exergy Analysis

An exergy and energy flow diagram for the baseline-case is given in Fig. 4 where energy flows are shown parenthetically on a HHV-basis (in MW) and exergy destructions within each subsystem are shown within brackets as a negative quantity. Overall, 467 MW of exergy in the form of biomass enter the plant and 205 MW of hydrogen exergy and 18.4 MW of net electrical energy are produced, yielding an overall exergetic (second-law) efficiency of 47.8%. The largest exergy destructions are found within the gasifier (117 MW), steam and power generation subsystem (~67 MW), pressure swing adsorption unit (~10.6 MW), and the water-gas shift reactors (~6 MW). Table 4 also provides an exergy accounting summary.

7.1 Gasifier. As the gasifier represents the largest single source of exergy destructions within the plant (25% of the total exergy entering in the form of biomass or 55% of the total exergy destroyed and lost within the plant), a more detailed analysis of the losses within it was made. Figure 5 shows an exergy/energy flow diagram that summarizes losses within the gasifier unit. About 117 MW of exergy are destroyed and/or lost within the gasifier. Heat loss from the gasifier is estimated at a 100°C surface temperature and amounts to only ~0.8 MW of exergy. The efficiency of the gasifier is estimated by

$$\eta_{\mathrm{II}} = \frac{\dot{\psi}_{\mathrm{syngas}}}{\sum \dot{\psi}_{\mathrm{in}}} = \frac{370.4}{467 + 2.9 + 1.1 + 18.4} = 75.7\%$$

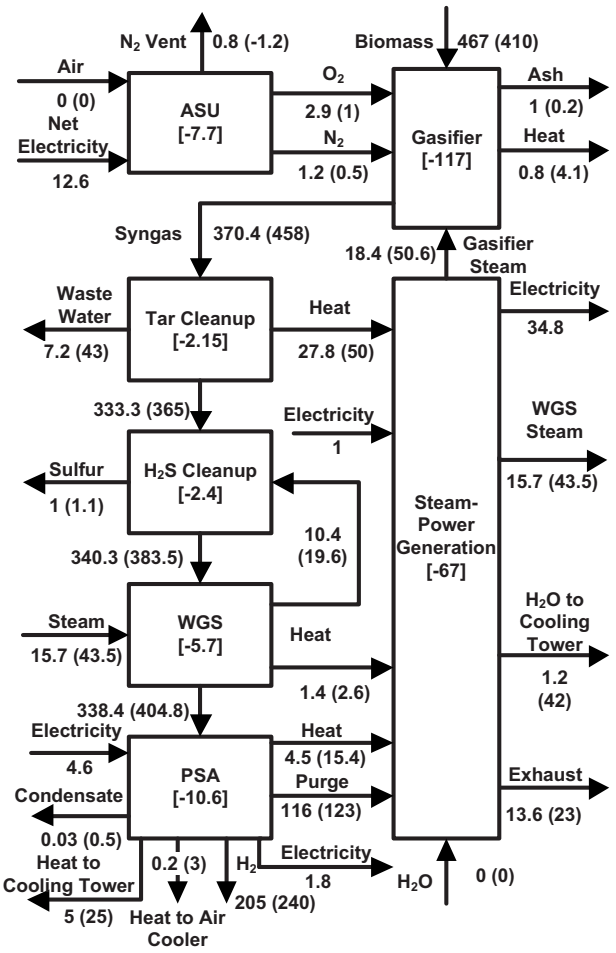

Fig. 4 Baseline-case exergy/exergy flow diagram

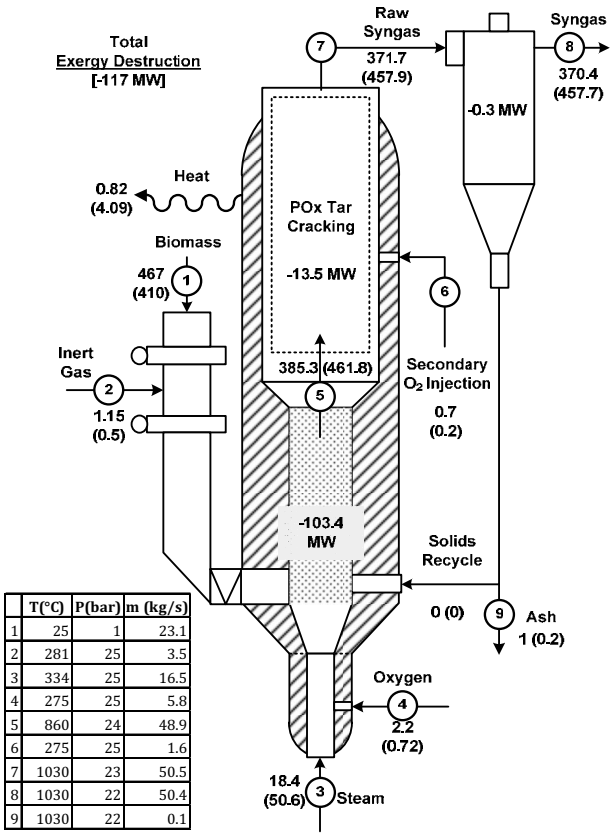

	T(°C)	P(bar)	m (kg/s)
1	25	1	23.1
2	281	25	3.5
3	334	25	16.5
4	275	25	5.8
5	860	24	48.9
6	275	25	1.6
7	1030	23	50.5
8	1030	22	50.4
9	1030	22	0.1

Fig. 5 Gasifier exergy/energy flow detail

This value is slightly lower than the gasifier cold-gas efficiency of 77.8%. The exergy of the H_2 and CO make up 37% of the total availability in the syngas, at 19.7% and 17.3%, respectively. Of the 103 MW of exergy destroyed within the gasifier, only about 2.2 MW are lost within the gasifier due to the mixing of the O_2 and steam in the fluidizing stream. Gasifier losses are dominated by the irreversibilities associated with the partial oxidation gasification reaction kinetics and heat transfer/mixing losses between reaction reactants and products. Additionally, tar cracking in the freeboard consumes 13.5 MW (11.4% of the total destroyed/lost) and particulate/ash removal only 0.3 MW.

Table 4 Exergy accounting summary

Exergy input	Baseline Case	% of total	Future Case	% of total
Biomass	467		467	
	Exergy output			
Electricity	18.4	3.9	30.4	6.5
Hydrogen	205.0	43.9	205.0	43.9
Water (cooling tower, condensate, etc.)	13.4	2.9	5.6	1.2
Sulfur	1.0	0.2	1.0	0.2
Other (ash, N_2 vent, heat, etc.)	16.4	3.5	17.6	3.8
Total	254.2	54.4	259.6	55.6
	Exergy destroyed			
Gasifier	117.3	25.1	117.3	25.1
Tar cleanup	2.2	0.5	0.4	0.1
H_2S cleanup	2.4	0.5	0.1	0.0
WGS	5.7	1.2	1.1	0.2
PSA	10.6	2.3	10.5	2.2
Steam+power	67.0	14.3	70.6	15.1
ASU	7.7	1.6	7.7	1.6
Total	212.8	45.6	207.6	44.4

7.2 Tar Cleanup. The tar in the syngas leaving the gasifier is converted to hydrogen and carbon monoxide in the reactors and the syngas is quenched from 693°C to 161°C prior to the wet scrubbing operation. The thermal energy from the quenching process is recovered and transferred to the steam cycle via a heat exchanger network. The overall efficiency of the tar cleanup process (from station (2) to downstream of the wet scrubber in Fig. 2) is given by,

$$\eta_{II} = \frac{\dot{\psi}_{syngas,out}}{\dot{\psi}_{syngas,in}} = \frac{333.3}{370.4} = 90\%$$

The tar compounds only compromise 1.45 MW of the 370 MW of exergy in the syngas stream. If the exergy associated with the thermal energy transfer to the steam cycle is included in the numerator, the second-law efficiency improves to 97.5%. The exergy destruction is largely due to the chemical transformations of tar within the reactors and direct contact mixing from cooling water injection in the quench process. The exergy destroyed due to heat transfer is accounted for in the steam-power production block.

7.3 H_2S Cleanup. Desulfurization of the syngas requires 10.4 MW of exergy in the form of process heat for reheat of the syngas stream to 375°C prior to the ZnO polishing beds. One output of the LO-CAT process is elemental sulfur suitable for export. While

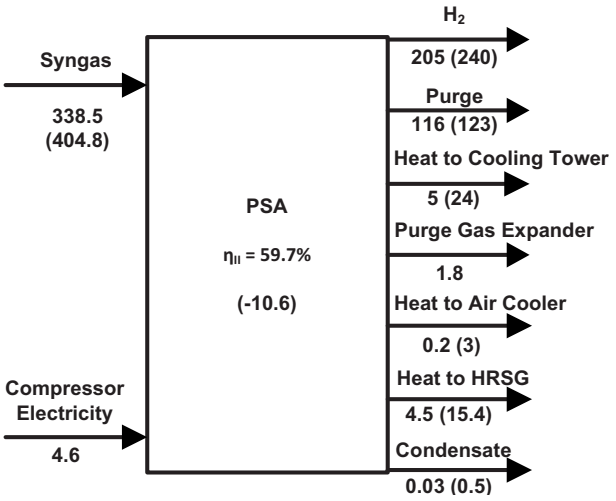

Fig. 6 Exergy/energy flow diagram of PSA unit

the captured sulfur has exergetic value, it is viewed as a waste stream in this process. The efficiency of the H_2S cleanup process is then given by

$$\eta_{II} = \frac{\dot{\psi}_{syngas,out}}{\dot{\psi}_{syngas,in} + \dot{\psi}_{heat}} = \frac{340.3}{333.3 + 10.4} = 99\%$$

The majority of the exergy destroyed in this subsystem occurs in the reheater for the ZnO polishing bed.

7.4 Water Gas Shift. Downstream of the desulfurization process, the CO in the syngas is shifted to CO_2 in the water-gas shift reactor train to increase H_2 content. This is to ensure that the maximum amount of H_2 is available in the syngas stream for recovery in the PSA unit. The efficiency for the WGS process is given by

$$\eta_{II} = \frac{\dot{\psi}_{syngas,out}}{\dot{\psi}_{syngas,in} + \dot{\psi}_{steam}} = \frac{338.5}{340.3 + 15.7} = 95\%$$

7.5 Hydrogen Purification. After two stages of water-gas shift, the H_2 content of the syngas is about 55% on a molar basis. For efficient recovery of H_2 in the PSA unit, the molar fraction should be greater than 70% [2] and therefore, a fraction of the product H_2 is recycled to the inlet. While recycle is employed, the H_2 mole fraction is only just above the required level which leads to lower recovery efficiency. This also contributes to the exergy destruction in this process. An exergy/energy flow diagram is given in Fig. 6.

The exergy of the purge stream is recaptured in the steam-power production process but is not considered in the second-law efficiency for the H_2 purification process. The efficiency for the H_2 purification process is given by,

$$\eta_{II} = \frac{\dot{\psi}_{H_2}}{\dot{\psi}_{syngas,in} + \dot{\psi}_{comp}} = \frac{205}{338.5 + 4.6} = 59.7\%$$

Inclusion of the exergy of the purge gas and the purge gas expander electricity increases the second-law efficiency to about 94% as given by,

$$\eta_{II} = \frac{\dot{\psi}_{H_2} + \dot{\psi}_{purge} + \dot{\psi}_{electricity}}{\dot{\psi}_{syngas,in} + \dot{\psi}_{comp}} = \frac{205 + 116 + 1.8}{338.5 + 4.6} = 94.1\%$$

7.6 Steam-Power Production. The purge gas and the process heat from the system are sent to the steam-power production subsystem. The purge gas is burned in a combustor and heat is recovered from the exhaust via a heat exchanger network. An exergy and energy flow diagram of the subsystem is given in Fig. 7 and includes the purge gas combustor.

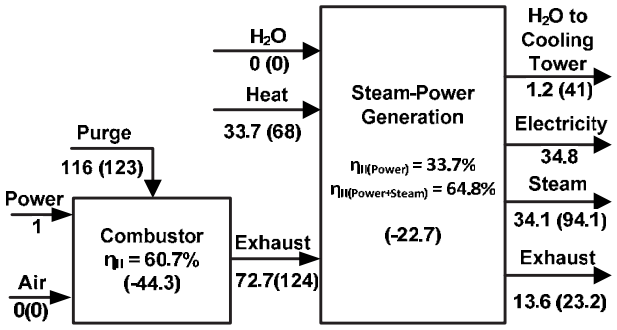

Fig. 7 Exergy/Energy flow diagram for steam-power generation process

The exhaust is vented to the atmosphere at 90°C and carries with it about 13.6 MW of exergy. Process steam in the plant is required for the gasifier and WGS reactors. Approximately 34 MW of steam are extracted from the intermediate pressure (25 bars) turbine in the plant. The efficiency of the steam-power generation process is given by,

$$\eta_{II} = \frac{\dot{\psi}_{electricity} + \dot{\psi}_{steam}}{\sum \dot{\psi}_{in}} = \frac{34.8 + 34.1}{72.7 + 33.7} = 68.9\%$$

Within the steam-power generation subsystem, the purge gas combustor is responsible for 44 MW (or ~66%) of the total exergy destroyed. About 6.5 MW of that destruction is associated with irreversible mixing of purge gas and combustion air. Over 92% of the destruction due to mixing is diffusional processes with the remainder due to heat transfer between reactants and products. Nearly 23 MW of exergy destruction is associated with heat transfer within the process steam generation heat exchanger network. If the second-law efficiency is examined as only a function of exportable power, the efficiency becomes

$$\eta_{II} = \frac{\dot{\psi}_{electricity}}{\sum \dot{\psi}_{in}} = \frac{34.8}{72.7 + 33.7} = 32.7\%$$

7.7 O_2 Production and Supply. The subsystem related to oxygen production and supply consists of the cryogenic air separation unit and the oxygen and nitrogen compressors for supply to the gasifier. Only a small fraction of the nitrogen produced in the ASU is required by the lock-hopper feeding system; thus, any nitrogen not required for pressurization is expanded and then vented to the atmosphere prior to compression. An exergy/energy flow diagram is given in Fig. 8.

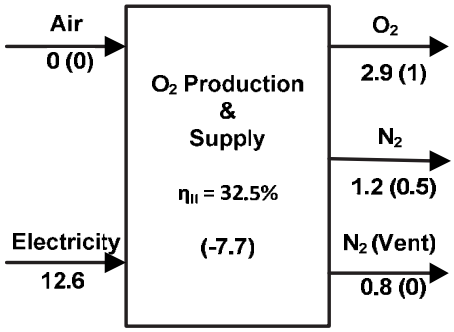

Fig. 8 Exergy/energy flow diagram for ASU

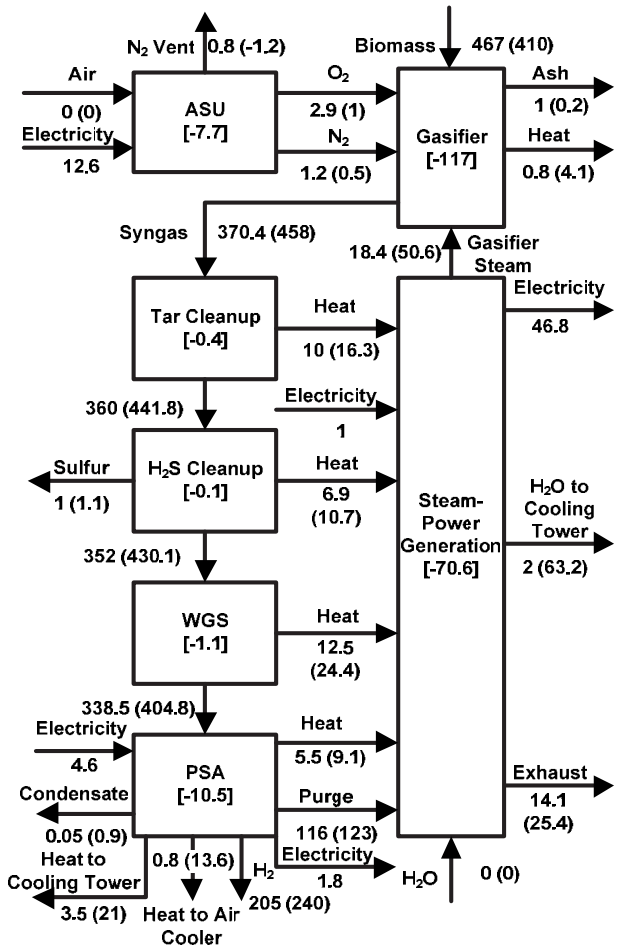

Fig. 9 Exergy/energy flows for future-case plant

The efficiency of the O_2 production and supply process is given by,

$$\eta_{II} = \frac{\dot{\psi}_{O_2} + \dot{\psi}_{N_2}}{\dot{\psi}_{electricity}} = \frac{2.9 + 1.2}{12.6} = 32.5\%$$

A detailed analysis of losses in air separation is not performed here, but according to Yong et al. [38], the majority of the exergy destroyed in air separation processes occurs in the heat exchangers (56%) and the distillation towers (23%). However, as previously discussed, a conservative electrical energy consumption per kg of oxygen produced was employed in the biorefinery. An optimistic value of 0.260 kW h/kg O_2 (rather than 0.35) would increase the second-law efficiency to a value of nearly 44% for the ASU achieving a performance gain of about 33% and an overall plant efficiency improvement of 0.8%.

8 Future-Case Exergy Analysis

An exergy flow diagram for the future-case is given in Fig. 9 and a table summary is also provided in Table 4. Overall, 467 MW of exergy in the form of biomass enter the plant and 205 MW of hydrogen exergy and 30.4 MW of net electrical energy are produced, yielding an overall exergetic (second law) efficiency of 50.4%. Compared with the baseline-case, the largest improvements in subsystem exergetic efficiency are achieved in the steam-power generation and PSA units. The gasifier and ASU subsystems are identical to the baseline case.

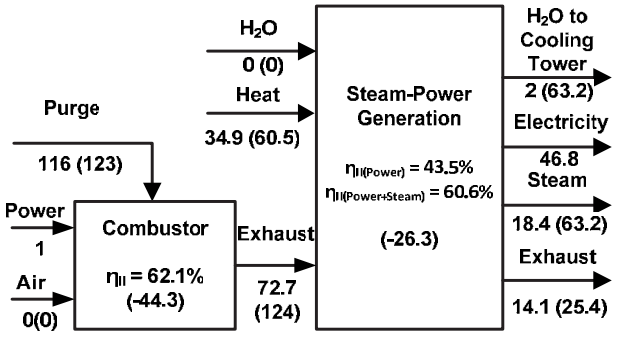

Fig. 10 Exergy/energy flows for future-case steam-power generation process

8.1 Tar Cleanup. The future-case tar cleanup reduces the amount of cooling that is required and shifts the exergy from the process heat stream to the syngas stream. This improves the η_{II} from 90% to 97.2%.

8.2 H_2S Cleanup. The future-case desulfurization process is a significant improvement over the baseline-case. The exergy destruction reduces from 2.4 MW to only 0.1 MW and rather than requiring process heat to reheat the stream, the future-case provides an additional 6.9 MW of availability as process heat for steam generation. The efficiency of the H_2S cleanup process is 97.8% and despite the decrease in exergy destruction would appear to be lower than the baseline-case. However, when the availability of the heat transferred to the steam plant is included, the second law efficiency improves to 99.7%.

8.3 Water Gas Shift. The elimination of the wet scrubbing step preserves the H_2O content in the syngas stream. This eliminates the need for steam injection before the WGS reactor train and leads to a significant increase in steam that is available for power production. The exergy destruction reduces from 5.7 MW to 1.1 MW. 96.1% exergetic efficiency for the WGS process is achieved.

8.4 H_2 Purification. The alterations in the syngas cleanup train result in a higher partial pressure of H_2, which slightly improves the efficiency of the PSA unit. The efficiency for the H_2 purification process is given by

$$\eta_{II} = \frac{205}{338.4 + 4.6} = 59.8\%$$

If the purge is included, the second-law efficiency jumps to

$$\eta_{II} = \frac{205 + 119}{338.4 + 4.6} = 94.5\%$$

This result is similar to the baseline-case. The improvement in the process is observed in the additional 1 MW of available energy delivered to the steam-power generation process.

8.5 Steam-Power Production. The largest improvements in system efficiency are achieved in the steam generation and power production subsystem. The use of emerging gas cleanup technologies enabled process improvements that primarily served to improve the thermal integration of the system. The improved thermal integration and reduction in process steam allows for an additional 12 MW of electricity to be produced for export, thereby raising the subsystem second-law efficiency from 35% to 46%. The increased amount of steam available for power production also increases the amount of heat transfer in the heating-cooling equipment in the steam-power system which results in a slight increase in exergy destroyed (70.6 MW versus 67 MW). An exergy/energy flow diagram that summarizes these results is given in Fig. 10.

9 Additional Suggestions for Improvement

The use of emerging gas cleanup technologies has been shown to offer plant energetic and exergetic efficiency gains of 2 percentage points or more. The removal of CO_2 prior to the water-gas shift and hydrogen purification steps proves to have a significant effect on pressure-swing adsorption effectiveness. The PSA requires a hydrogen molar concentration of about 70% at the inlet; thus, in both the future and baseline cases, product hydrogen recycle is required as shown in Figs. 2 and 3. A high-level analysis was performed to investigate the effect of CO_2 removal from the syngas on overall fuel production efficiency. The removal of H_2S and CO_2 constituents from the syngas at a location downstream of the tar removal processes was investigated by approximation of a two-stage Selexol-type unit. A portion of the captured CO_2 is fed to the lock-hopper system and serves as the feedstock pressurizing agent, while nitrogen from the ASU is no longer needed and is expanded and vented to the atmosphere. This preliminary analysis found that a higher overall plant efficiency may be achieved if carbon dioxide is removed upstream of the shift and purification processes. The performance gain is due in part to the fact that CO_2 removal produces a syngas with a substantially higher hydrogen partial pressure, which ultimately allows for much greater recovery of the hydrogen in the PSA unit ($\sim$92% versus 71%). However, higher hydrogen concentration at the inlet to the PSA results in a lower calorific value gas that is sent to the purge gas combustor, which translates into a reduction in steam generation and net plant power production. Thus, total plant efficiency improvements are subject to a trade-off in the reduction in the electrical generation efficiency versus the net hydrogen production efficiency. Refinery capital cost is estimated to increase by about 10% due to the addition of the Selexol plant for CO_2 removal. A more detailed techno-economic analysis is required but a preliminary assessment indicates that removal of CO_2 may offer a compelling case for implementing CO_2 capture even in the absence of significant carbon emission legislation.

10 Conclusions

Comparative analyses of two conceptual 2000 tPD thermochemical-based biorefineries for the production of hydrogen and electricity were performed using system models created in ASPEN Plus®. The models were used to make thermodynamic evaluations of near-term and future biorefinery concepts, with an emphasis on exploration of the effects of emerging technologies on process efficiencies. The baseline-case was estimated to achieve a fuel conversion efficiency of 58.8% HHV and a total efficiency of 63.2% HHV. The future-case concept predicts the fuel and total efficiencies of 58.6% and 65.3%, respectively. The areas of greatest exergy destruction identified by this analysis are (i) gasification, (ii) steam/power production, and (iii) gas purification process. The 2 percentage point improvement in exergetic efficiency between baseline and future cases was made possible by tighter thermal integration of gas cleanup and process steam generation processes. The greatest destroyers of exergy identified in this study provide good focus areas for further research and development. In the hydrogen purification portion of the plant, the inefficiencies are due primarily to the dilute nature of the syngas. Without CO_2 capture, the more dilute syngas results in lower overall recovery of hydrogen by the PSA unit. Preliminary analysis suggests that removing the CO_2 in the syngas early in the process and switching the pressurizing agent to CO_2 from N_2 by employing technologies such as Selexol, Rectisol, or membrane reactors prior to hydrogen purification would substantially improve hydrogen recovery and offer a net gain in total plant efficiency. It was also recognized that a 25% more efficient ASU could increase total plant efficiency by about 0.8% from the baseline system value.

Acknowledgment

The authors would like to acknowledge the Institute of Transportation Studies at University of California-Davis for partial support of this research.

Nomenclature

ψ_p = physical exergy (kJ/kmol)
ψ_{ch} = chemical exergy (kJ/kmol)
$\dot{\psi}$ = exergy flow (kW)
$\bar{h}_{T,P}$ = specific molar enthalpy at T, P (kJ/kmol)
$\Delta\bar{h}$ = change in specific molar enthalpy (kJ/kmol)
$\bar{s}_{T,P}$ = entropy at T, P (kJ/kmol-K)
$\Delta\bar{s}$ = change in specific molar entropy (kJ/kmol K)
$\bar{R}$ = universal gas constant (kJ/kmol K)
T_o = environmental temperature (298.15 K)
P_i = partial pressure of ith component (bar)
y_i = mole fraction of ith component
η_{II} = second-law efficiency
LHV = lower heating value (MJ/kg)
HHV = higher heating value (MJ/kg)

References

[1] Larson, E. D., Jin, H., and Celik, F. E., 2009, "Performance and Cost Analysis of Future, Commercially Mature Gasification Based Electric Power Generation From Switchgrass," Biofuels. Bioprod. Bioref., **3**, pp. 174–194.
[2] Spath, P., Aden, A., Eggeman, T., Ringer, M., Wallace, B., and Jechura, J., 2005, "Biomass to Hydrogen Production Detailed Design and Economics Utilizing the Battelle Columbus Laboratory Indirectly-Heated Gasifier," National Renewable Energy Laboratory Report No. TP-510-37408.
[3] Williams, R., Larson, E., Katofsky, R., and Chen, J., 1995, "Methanol and Hydrogen From Biomass for Transportation," Energy for Sustainable Development, **1**, pp. 18–34.
[4] Corradetti, A., and Desideri, U., 2007, "Should Biomass Be Used for Power Generation or Hydrogen Production?," ASME J. Eng. Gas Turbines Power, **129**, pp. 629–635.
[5] Dean, J., Braun, R., Munoz, D., Penev, M., and Kinchin, C., 2010, "Analysis of Hybrid Hydrogen Systems—Final Report," National Renewable Energy Laboratory Report No. TP-46934.
[6] Dean, J., Braun, R., Munoz, D., Penev, M., and Kinchin, C., 2010, "Leveling Intermittent Renewable Energy Production Through Biomass Gasification-Based Hybrid Systems," Proceedings of the ASME 2010 Fourth International Conference on Energy Sustainability, ES2010, Phoenix, AZ, May 17–21.
[7] Phillips, S., Aden, A., Jechura, J., Dayton, D., and Eggeman, T., 2007, "Thermochemical Ethanol via Indirect Gasification and Mixed Alcohol Synthesis of Lignocellulosic Biomass," National Renewable Energy Laboratory Technical Report No. NREL/TP-510-41168.
[8] Dutta, A., and Phillips, S., 2009, "Thermochemical Ethanol via Direct Gasification and Mixed Alcohol Synthesis of Lignocellulosic Biomass," National Renewable Energy Laboratory Technical Report No. NREL/TP-510–45913.
[9] Rodriguez, L., and Gaggioli, R. A., 1980, "Second-Law Efficiency of a Coal Gasification Process," Can. J. Chem. Eng., **58**(3), pp. 376–381.
[10] Singh, S. P., Weil, S. A., and Babu, S. P., 1980, "Thermodynamic Analysis of Coal Gasification Processes," Energy, **5**, pp. 905–914.
[11] Srinivas, T., Gupta, A.V., Reddy, B.V., 2009, "Thermodynamic Equilibrium Model and Exergy Analysis of a Biomass Gasifier," ASME J. Energy Resour. Technol., **131**, p. 031801.
[12] Ptasinski, K. J., Prins, M. J., and Pierik, A., 2007, "Exergetic Evaluation of Biomass Gasification," Energy, **32**, pp. 568–574.
[13] Prins, M. J., Ptasinski, K. J., and Janssen, F. J., 2007, "From Coal to Biomass Gasification: Comparison of Thermodynamic Efficiency," Energy, **32**, pp. 1248–1259.
[14] Milne, T., and Evans, R., 1998, "Biomass Gasifier Tars: Their Nature, Formation, and Conversion," National Renewable Energy Laboratory Technical Report No. NREL/TP-570-25357.
[15] Milbrandt, A., 2005, "Geographic Perspective on the Current Biomass Resource Availability in the United States," National Renewable Energy Laboratory Report No. TP-560-39181.
[16] Perlack, R., Wright, L., Turhollow, A., Graham, R., Stokes, B., and Erbach, D., 2005, "Biomass as Feedstock for a Bioenergy and Bioproducts Industry: The Technical Feasibility of a Billion-Ton Annual Supply," Oak Ridge National Laboratory.
[17] Phyllis Biomass Datapage, "Wood, Hybrid Poplar," ID No. 806, www.ecn.nl/phyllis, accessed October 2008.
[18] Parker, N., Tittmann, P., Hart, Q., Lay, M., Cunningham, J., Jenkins, B., Nelson, R., Skog, K., Milbrandt, A., Gray, E., and Schmidt, A., 2008, "Strategic Assessment of Bioenergy Development in the West: Spatial Analysis and Sup-

ply Curve Development," Final Report to the Western Governor's Association, prepared by the University of California-Davis, Sept.
[19] Parker, N., 2007, "Optimizing the Design of Biomass Hydrogen Supply Chains Using Real-World Spatial Distributions: A Case Study Using California Rice Straw," *Transportation Technology and Policy*, Institute of Transportation Studies, University of California-Davis, Davis, CA.
[20] Aravind, P. V., Woudstra, T., Woudstra, N., and Spliethoff, H., 2009, "Thermodynamic Evaluation of Small-Scale Systems With Biomass Gasifiers, Solid Oxide Fuel Cells With Ni/GDC Anodes and Gas Turbines," J. Power Sources, **190**, pp. 461–475.
[21] Brown, D., Gassner, M., Fuchino, T., and Marechal, F., 2009, "Thermo-Economic Analysis for the Optimal Conceptual Design of Biomass Gasification Energy Conversion Systems," Appl. Therm. Eng., **29**, pp. 2137–2152.
[22] Higman, C., and van der Burgt, M., 2008, *Gasfication*, 2nd ed., Gulf Professional, Burlington, MA.
[23] Bolhar-Nordenkampf, M., and Hofbauer, H., 2004, "Gasification Demonstration Plants in Austria," International Slovak Biomass Forum, Bratislava, Feb. 9–10.
[24] Evans, R., Knight, R., Onishak, M., and Babu, S., 1998, "Development of Biomass Gasification to Produce Substitute Fuels," A Report Prepared by the Institute of Gas Technology for Pacific Northwest Laboratory.
[25] Pan, Y., Roca, X., Velo, E., and Puigjaner, L., 1999, "Removal of tar by secondary air in fluidized bed gasification of residual biomass and coal," Fuel, **78**, pp. 1703–1709.
[26] Bain, R., 1992, *Material and Energy Balances for Methanol from Biomass Using Biomass Gasifiers*, National Renewable Energy Laboratory.
[27] Hamelinck, C., Faaij, A., Uil, H., and Boerrigter, H., 2004, "Production of FT Transportation Fuels From Biomass; Technical Options, Process Analysis and Optimisation, and Development Potential," Energy, **29**, pp. 1743–1771.
[28] American Water Works Association & American Society of Civil Engineers, 1997, *Water Treatment Plant Design*, 3rd ed., McGraw-Hill, New York.
[29] Smith, A., and Klosek, J., 2001, "A Review of Air Separation Technologies and their Integration With Energy Conversion Processes," Fuel Process. Technol., **70**, pp. 115–134.
[30] Wang, W., Padban, N., Ye, Z., Olofsson, G., Andersson, A., and Bjerle, I., 2000, "Catalytic Hot Gas Cleaning of Fuel Gas From an Air-Blown Pressurized Fluidized-Bed Gasifier," Ind. Eng. Chem. Res., **39**, pp. 4075–4081.
[31] Kemp, I., 2007, *Pinch Analysis and Process Integration*, 2nd ed., Butterworth, Washington, DC/Heinemann, London.
[32] Engelen, K., Zhang, Y., Draelants, D., and Baron, G., 2005, "A Novel Catalytic Filter for Tar Removal From Biomass Gasification Gas: Improvement of the Catalytic Activity in Presence of H_2S ," Renewable Energy, **20**, pp. 565–587.
[33] Nexant, Inc., 2007, "Preliminary Feasibility Analysis of RTI Warm Gas Cleanup (WGCU) Technology," Prepared for the Research Triangle Institute (RTI), Jun.
[34] Moran, M. J., 1989, *Availability Analysis*, ASME, New York.
[35] Moran, M. J., and Shapiro, H. N., 2008, *Fundamentals of Engineering Thermodynamics*, 6th ed., Wiley, Hoboken, NJ.
[36] Szargut, J., 2005, *Exergy Method Technical and Ecological Applications*, WIT Press, Ashurst Lodge, Southhampton, UK.
[37] Szargut, J., Morris, D. R., and Steward, F. R., 1988, *Exergy Analysis of Thermal, Chemical, and Metallurgical Processes*, Hemisphere, New York.
[38] Yong, P., Moon, H., and Yi, S., 2002, "Exergy Analysis of Cryogenic Air Separation Process for Generating Nitrogen," Ind. Eng. Chem., **8**(6), pp. 499–505.